HOKKAIDO UNIVERSITY

Title	Update on the 53Mn-53Cr ages of dolomite in the Ivuna CI chondrite and asteroid Ryugu sample
Author(s)	Sugawara, Shingo; Fujiya, Wataru; Kawasaki, Noriyuki et al.
Citation	Geochimica et cosmochimica acta, 382, 40-50 https://doi.org/10.1016/j.gca.2024.08.013
Issue Date	2024-10-01
Doc URL	https://hdl.handle.net/2115/97267
Rights	© 2024. This manuscript version is made available under the CC-BY-NC-ND 4.0 license http://creativecommons.org/licenses/by-nc-nd/4.0/
Rights(URL)	https://creativecommons.org/licenses/by-nc-nd/4.0/
Type	journal article
File Information	Sugawara_IvunaMnCr_GCA.pdf

Hokkaido University Collection of Scholarly and Academic Papers

Hokkaido University Collection of Scholarly and Academic Papers : HUSCAP

Update on the ^{53}Mn-^{53}Cr ages of dolomite in the Ivuna CI chondrite and asteroid Ryugu sample

Shingo Sugawara[1], Wataru Fujiya[1,*], Noriyuki Kawasaki[2], Naoya Sakamoto[3], Akira Yamaguchi[4], and Hisayoshi Yurimoto[2]

[1]Faculty of Science, Ibaraki University, 2-1-1 Bunkyo, Mito, Ibaraki 310-8512, Japan.

[2]Department of Natural History Sciences, Hokkaido University, Sapporo 060-0810, Japan.

[3]Isotope Imaging Laboratory, Creative Research Institution, Hokkaido University, Sapporo 001-0021, Japan.

[4]National Institute of Polar Research, Midoricho10-3, Tachikawa, Tokyo 190-8518, Japan.

*Corresponding author (wataru.fujiya.sci@vc.ibaraki.ac.jp)

Under revision for publication in *Geochimica et Cosmochimica Acta*

Abstract

Aqueous alteration in planetesimals is one of the earliest geological processes in the solar system. The timing of aqueous alteration sheds light on the timescale of material evolution through water-rock interaction in small bodies. The ^{53}Mn-^{53}Cr decay system, where a short-lived radionuclide ^{53}Mn decays to ^{53}Cr with a half-life of 3.7 Myr, is a powerful tool for dating carbonates in primitive meteorites that formed during aqueous alteration. In CI chondrites and samples returned from asteroid Ryugu, a major carbonate mineral is dolomite ($CaMg(CO_3)_2$) and could be dated precisely because of their relatively high Mn abundances. However, the lack of a proper dolomite standard for secondary ion mass spectrometry (SIMS) hinders us from obtaining accurate Mn/Cr ratios of carbonates, resulting in erroneous formation ages. In this work, we synthesized Mn-, Cr-, and Fe-bearing crystalline dolomite as standard materials and evaluated the relative sensitivity factor (RSF) of Mn/Cr for SIMS analysis, namely, the ratio of Mn/Cr obtained using SIMS to true Mn/Cr. We found that the RSF values of the dolomite standards range from 0.8 to 0.9, slightly higher than that of calcite ($CaCO_3$) (~0.7), and increase with their Fe contents. We used the newly evaluated RSF values to date dolomite in the Ivuna CI chondrite and obtained an initial ^{53}Mn/^{55}Mn ratio of $(3.95 \pm 0.49) \times 10^{-6}$ (95% confidence interval) and the corresponding absolute age of 4564.0 +0.6/−0.7 Ma. Our new initial ^{53}Mn/^{55}Mn ratio is 26 ± 19% higher than that obtained by a previous study for the same dolomite grain using a calcite standard. This difference is consistent with the difference between the RSF values of dolomite and calcite. Based on these results, we updated the initial ^{53}Mn/^{55}Mn ratio previously reported for dolomite in the Ryugu sample A0058 to be $(3.21 \pm 0.66) \times 10^{-6}$, which corresponds to an absolute age of 4562.8 +1.0/−1.2 Ma. This age seems to be the best estimate for the formation age of dolomite in Ryugu

currently available.

Keywords: ^{53}Mn-^{53}Cr dating; Carbonate; SIMS; Standard material; Relative sensitivity factor

1. Introduction

Chondrites are a group of meteorites that did not undergo large-scale melting/differentiation in their parent bodies and have essentially unfractionated chemical compositions (except for highly volatile elements) from the solar composition (e.g., Weisberg et al., 2006). Among them, Ivuna-like (CI), Mighei-like (CM), and Renazzo-like (CR) chondrites as well as some ungrouped carbonaceous chondrites such as Tagish Lake are samples rich in water and organic matter, and as a result, volatile elements such as H, C, and N (e.g., Grady and Wright, 2003; Alexander et al., 2012). These meteorite groups are thus "chemically" primitive, however, they are also meteorite groups whose constituents are most severely influenced by aqueous alteration, i.e., water-rock interaction, in their parent bodies (e.g., Brearley, 2006; Krot et al., 2015).

A variety of secondary minerals such as phyllosilicates, oxides, sulfides, and carbonates formed during aqueous alteration by either precipitation from aqueous solutions or replacement of other minerals. The alteration degrees, i.e., to what extent primary minerals disappeared and secondary minerals formed, are expressed by petrologic types from 3 to 1. CI chondrites are all classified as type 1 and largely composed of Fe-bearing, Mg-rich serpentine and smectite matrix (e.g., Tomeoka and Buseck, 1988; Zolensky et al., 1993). Other constituents of CI chondrites include magnetite: Fe_3O_4, carbonates (mainly dolomite: $CaMg(CO_3)_2$, and less abundant calcite: $CaCO_3$ and breunnerite: $(Mg,Fe,Mn)CO_3$), and sulfides (pyrrhotite: $Fe_{1-x}S$ and pentlandite: $(FeNi_9)S_8$) (e.g., Endress and Bischoff, 1996; Hua and Buseck, 1998; Bullock et al., 2005; King et al., 2015; Schrader et al., 2021).

Aqueous alteration is one of the earliest geological processes operating in the early solar

system, and the liquid water was available through heating of ice accreted by the meteorite parent bodies. Macdougall and Lugmair (1984) first suggested early aqueous activity in the CI parent body within 100 Myr after the formation of the oldest solids in the solar system (Ca- and Al-rich inclusions: CAIs), based on ^{87}Rb-^{87}Sr isotope systematics of carbonate and sulfate which precipitated from aqueous solutions. Much tighter constraints on the timing of aqueous activity have been put by using a short-lived radionuclide ^{53}Mn which decays to ^{53}Cr with a half-life of 3.7 Myr. A pioneering work by Endress et al. (1996) performed ^{53}Mn-^{53}Cr dating of carbonates, which preferentially incorporated Mn over Cr, in the Orgueil and Ivuna CI chondrites using secondary ion mass spectrometry (SIMS). They detected elevated ^{53}Cr/^{52}Cr ratios that correlate with ^{55}Mn/^{52}Cr ratios indicating *in-situ* decay of ^{53}Mn. The inferred initial ^{53}Mn/^{55}Mn ratio, $(^{53}Mn/^{55}Mn)_0$, at the closure of Mn-Cr isotopes is 1.99×10^{-6}, and they concluded that aqueous alteration in the CI parent body must have begun <20 Myr after CAIs. The early aqueous alteration points to an idea that the decay energy of short-lived radionuclides such as ^{26}Al (half-life: 0.7 Myr) caused melting of ice and liquid water available (e.g., Grimm and McSween, 1989; Cohen and Coker, 2000). From this point of view, the ages of carbonates are crucial for elucidating the accretion time and thermal history of chondrite parent bodies because the accretion time predominantly determined the amount of incorporated ^{26}Al as a heat source.

Because dolomite is a major carbonate mineral in CIs and can incorporate a substantial amount of Mn, previous studies of Mn-Cr dating for CIs have focused on dolomite, although some studies analyzed breunnerite as well (Endress et al., 1996; Hoppe et al., 2007; Fujiya et al., 2013; Steele et al., 2017; Visser et al., 2020). Previous studies also measured the Mn-Cr ages of dolomite (and minor calcite and breunnerite) in samples

from asteroid Ryugu, which were returned by JAXA's Hayabusa2 spacecraft and resemble CIs (Nakamura et al., 2022; Yokoyama et al., 2023a; McCain et al., 2023). These previous studies have obtained variable $(^{53}Mn/^{55}Mn)_0$, and thus, Mn-Cr ages. For Ryugu dolomite, the highest $(^{53}Mn/^{55}Mn)_0$ ratio of $(6.8 \pm 0.5) \times 10^{-6}$ was reported by McCain et al. (2023), while the lowest value of $(2.55 \pm 0.35) \times 10^{-6}$ was obtained by Yokoyama et al. (2023a). At face value, the variation in $(^{53}Mn/^{55}Mn)_0$ corresponds to a time span of ~5.2 Myr, and thus, suggesting a prolonged formation of dolomite for at least 5 Myr.

However, a caveat should be taken for analytical techniques of Mn-Cr dating using SIMS. $(^{53}Mn/^{55}Mn)_0$ is calculated from the slope of the regression line of data in a $^{53}Cr/^{52}Cr$ vs. $^{55}Mn/^{52}Cr$ space, so-called isochron diagram. The instrumental fractionation between true ratios and secondary ion intensity ratios are empirically corrected using a standard material with known $^{53}Cr/^{52}Cr$ and $^{55}Mn/^{52}Cr$ ratios. In case of SIMS, the instrumental fractionation is known to be dependent on matrix, i.e., the chemical composition and crystal structure of a sample, and therefore, we must use a proper matrix-matched standard for SIMS analysis. This is known as the matrix effect. The instrumental fractionation of isotope ratios, e.g., $^{53}Cr/^{52}Cr$, is no more than a few % in most cases, on the other hand, fractionation between different elements, e.g., $^{55}Mn/^{52}Cr$, can change drastically depending on the mineral species and chemical compositions of samples. For example, Doyle et al. (2015) reported that the relative sensitivity factor (RSF) of $^{55}Mn/^{52}Cr$, defined by $(^{55}Mn^+/^{52}Cr^+)_{SIMS}/(^{55}Mn/^{52}Cr)_{true}$, increases from ~0.9 to ~1.6 with increasing Fe contents in olivine. Sugiura et al. (2010) also pointed out that the Mn/Cr RSF value of calcite is lower than that of olivine by up to 30%. These previous studies strongly suggested an importance of using a proper, matrix-matched standard for Mn-Cr

dating of carbonate and olivine.

A problem is that natural carbonate contains little amount of Cr, and thus, it is difficult to prepare a carbonate standard with a known Mn/Cr ratio to evaluate the Mn/Cr RSF value. This situation led Sugiura et al. (2010) to produce a synthetic calcite doped with Mn and Cr from a solution, and they evaluated the Mn/Cr RSF value of calcite, as described above. Fujiya et al. (2012) first measured the Mn-Cr ages of calcite in CMs using this synthetic calcite standard. It should be noted that, however, most Mn-Cr ages of dolomite have also been measured using a synthetic calcite or San Carlos olivine standard, i.e., without using a dolomite standard (Endress et al., 1996; Hoppe et al., 2007; Fujiya et al., 2013; Visser et al., 2020; Nakamura et al., 2022; Yokoyama et al., 2023a). Therefore, the Mn-Cr ages measured by these studies are likely biased. Because the kinetics of dolomite crystallization is extremely slow, laboratory synthesis of dolomite under ambient conditions has not been successful. This is known as the dolomite problem (e.g., Land, 1998; Warren, 2000; Holland and Zimmermann, 2000; Pina et al., 2020), and thus, the preparation of a dolomite standard with a known Mn/Cr ratio seems much more difficult than calcite. Another approach for the preparation of a dolomite standard is Cr-ion implantation into natural dolomite (Steele et al., 2017; McCain et al., 2020). This would be an ingenious approach because we can dose an arbitrary amount of Cr, and these authors suggested that the RSF values of carbonates are dependent on their Fe contents. However, ion implantation inevitably results in non-uniform distribution of Cr in a depth direction. Therefore, it is not easy to analyze Cr-implanted standards and unknown samples under the same conditions. The two highest $(^{53}Mn/^{55}Mn)_0$ ratios among the extraterrestrial samples were both obtained using Cr-implanted carbonate standards (Steele et al., 2017; McCain et al., 2023), and the validity of this approach and the

accuracy of these values need to be addressed.

In this study, we synthesized crystalline dolomite by heating amorphous carbonate, rather than direct precipitation from a solution, and doped Mn, Cr, and Fe to the synthetic dolomites. We then found that the Mn/Cr RSF values were inconsistent between the synthetic dolomites and the Cr-implanted dolomites. Finally, we applied the newly evaluated RSF values to obtain an accurate Mn-Cr age of Ivuna dolomite and tried updating the Mn-Cr age of Ryugu dolomite previously analyzed.

2. Materials and Methods

2.1. Dolomite synthesis

In the previous work by Sugawara et al. (2022), the crystalline dolomite was successfully produced by heating amorphous Ca- and Mg-carbonate (ACMC). Because dolomite is thermodynamically unstable at temperatures higher than 400 °C in the atmosphere, Sugawara et al. (2022) heated ACMC in a closed system filled with CO_2 of >1.2 bar at 420 °C. At this temperature, ACMC can crystallize to dolomite in a reasonable timescale within days. We applied this method to synthesize Mn-, Cr- and Fe-bearing crystalline dolomite. Because amorphous carbonate has a flexible structure, it can incorporate incompatible elements such as Cr.

First, we produced Mn-, Cr- and Fe-bearing ACMC by mixing 0.2 M Na_2CO_3 (10 ml) and 0.2 M $(Ca+Mg+Mn+Cr+Fe)Cl_2$ (10 ml) solutions. Because ACMC preferentially incorporate Ca over Mg, the Mg/Ca (mol/mol) ratio of the solution was set to be from 2.2 to 2.4 (Radha et al., 2012; Purgstaller et al., 2019; Montes-Hernandez et al., 2020). After

mixing, ACMC immediately precipitated from the highly supersaturated solution. We isolated the precipitate from the solution using a membrane filter (0.45 μm) under vacuum, and then, the precipitate was washed with acetone and dried in a vacuum desiccator (~0.02 MPa). Because the ACMC contained a substantial amount (20-30 wt%) of water, we then dehydrated the ACMC in a vacuum chamber (~1 Pa) at 270 °C. Sugawara et al. (2022) showed that the dehydration of ACMC completes until 310 °C but its decomposition begins above similar temperature.

Then, we heated the dehydrated ACMC in a heat- and pressure-resistant canister. Because Fe-bearing dolomite decomposes at even lower temperatures than pure dolomite, we filled the canister with high-pressure CO_2 gas. First, we put the ACMC in the canister and evacuated. Then, we cooled the canister with liquid N_2 and introduced 99.9% purity CO_2 gas to the container so that CO_2 gas condensed in the container. Next, we closed a valve and kept the canister at room temperature, and CO_2 ice evaporated. Finally, we heated the container at 300-340 °C and adjusted pressure at 35-50 bar for 2-3 days. The temperature and pressure were determined empirically through trial-and-error operations. After heating, we washed the experimental products with ultra-pure water to dissolve any impurities.

Because the synthetic dolomites are powder with a size from 10s to 100s nanometers (Sugawara et al., 2022), we pressed them at pressure of ~800 MPa to produce pellets. The pellets of the synthetic dolomites and a calcite similarly synthesized via amorphous Ca-carbonate (ACC) (Saito et al., 2020; Miyajima et al., 2020) were mounted together in epoxy and polished. We coated the surface of the polished mount with C for scanning electron microscope (SEM) observation and electron probe microanalyzer (EPMA)

185 analysis. We produced three synthetic dolomites with no Fe, ~2 mol% Fe (in total cations),
186 and 6 mol% Fe, and hereafter, these synthetic dolomites are referred to as Dol#0, Dol#2,
187 and Dol#6. The synthetic calcite, which has no Fe, is referred to as Cal#0.

188

189 *2.2. X-ray diffraction analysis of experimental products*

190 We performed X-ray diffraction (XRD) analysis to confirm that the ACMC still remained
191 amorphous after dehydration and that it crystallized to dolomite after heating at 300-
192 340 °C. The XRD analysis was performed using Rigaku Miniflex 600 at Ibaraki
193 University. We used a Si zero-background sample holder and calibrated peak positions
194 using NIST SRM 640f Si standard. We used SmartLab Studio II software for data
195 reduction and crystallographic open database (COD) files for phase identification and
196 indexing of the analyzed samples.

197

198 *2.3. Quantitative analysis of chemical compositions of synthetic dolomites*

199 We observed the synthetic dolomites and calcite in the polished mount using a field
200 emission-scanning electron microscope (FE-SEM: HITACHI S-4800 at Ibaraki
201 University). Then, we measured the chemical compositions of the synthetic dolomites
202 and calcite using EPMA (JEOL JXA-8200) at National Institute of Polar Research (NIPR),
203 Japan. The analyzed elements are Na, Mg, Cl, Ca, Cr, Mn, and Fe, and standard materials
204 used are jadeite (Na), olivine (Mg), tugtupite (Cl), calcite (Ca), chromite (Cr), spessartine
205 (Mn), Fe_2O_3 (Fe). To mitigate sample damage, we used a defocused electron beam of ~5
206 nA in current and ~10 μm in diameter, and the measurement time was limited to 60

seconds on peak tops (and 30 seconds for background). The acceleration voltage was 15 kV. To reduce statistical uncertainty, we repeated the analysis at approximately 200-600 spots throughout the pellet samples. The typical detection limits were 0.02 wt% (Na_2O), 0.02 wt% (MgO), 0.01 wt% (Cl), 0.02 wt% (CaO), 0.06 wt% (Cr_2O_3), 0.03 wt% (MnO), and 0.03 wt% (FeO). We omitted a few data beyond three standard deviation (3σ) from the average.

2.4. Evaluation of the RSF values and its application to Mn-Cr dating of dolomite in Ivuna

We then evaluated the RSF values of the synthetic dolomites and calcite for SIMS. Before the SIMS analysis, we coated the surface of the sample mount with Au. We performed Mn-Cr isotope analysis using Cameca ims 1280-HR at Hokkaido University with the analytical settings identical to those of Yokoyama et al. (2023a) except that we used an $^{16}O_2^-$ primary ion beam from Hyperion radiofrequency (RF) ion source (4-5 μm in diameter and ~50 pA in current) instead of an $^{16}O^-$ primary beam from a duoplasmatron ion source (5 μm in diameter and ~100 pA in current). The SIMS measurement was done for four days. Secondary ions of $^{52,53}Cr^+$ and $^{55}Mn^+$ produced by the primary ion beam were simultaneously detected with three electron multipliers (EMs). The mass resolution of $M/\Delta M$ was ~6800, enough to separate $^{53}Cr^+$ from $^{52}Cr^1H^+$ interference. The measurement time, which is particularly important as described below, was ~3600 seconds (120 cycles for 30 seconds/cycle) after 250 seconds pre-sputtering (scanning over 10 × 10 μm^2 areas with a 1 nA primary ion beam). We repeated the analysis a few times in a day for each synthetic dolomite and calcite to evaluate the external reproducibility.

As a reference, we analyzed San Carlos olivine as well.

We calculated the RSF value in each measurement from an observed $^{55}Mn^{+}/^{52}Cr^{+}$ ratio divided by the $^{55}Mn/^{52}Cr$ ratio measured using EPMA (we assumed the terrestrial isotopic abundance of ^{52}Cr). The $^{55}Mn^{+}/^{52}Cr^{+}$ ratios were calculated by summing up the $^{55}Mn^{+}$ and $^{52}Cr^{+}$ ion intensities throughout a measurement (i.e., using total $^{55}Mn^{+}$ and $^{52}Cr^{+}$ counts) rather than by averaging $^{55}Mn^{+}/^{52}Cr^{+}$ ratios in each cycle to minimize a systematic bias (Ogliore et al., 2011).

As an application of the newly evaluated RSF values, we measured the Mn-Cr age of dolomite in the Ivuna CI chondrite. It should be emphasized that special cares were taken for keeping the same analytical conditions as that for the dolomite standards because the observed $^{55}Mn^{+}/^{52}Cr^{+}$ ratios changed during a single analysis with sputtering time (see section 3.3). A dolomite grain analyzed here, Ivuna-H2 dolomite #7, is the same grain as that reported by Yokoyama et al. (2023a) so that we can directly compare our results obtained using the new dolomite standards to that obtained by Yokoyama et al. (2023a) using a calcite standard. We also analyzed another dolomite grain, Ivuna-H2 dolomite #3 that was newly analyzed. We stopped analyses if we met a sudden increase of $^{52}Cr^{+}$ counts. These analyses were normally associated with inclusions in the dolomites, which we found by later inspection of the SIMS pits with a SEM. The instrumental mass fractionation (IMF) of $^{53}Cr/^{52}Cr$ ratios was corrected assuming the terrestrial $^{53}Cr/^{52}Cr$ ratio of 0.113459 (Papanastassiou, 1986) for the synthetic carbonates, and we found that it was approximately −22‰, consistent with that reported by Sugiura et al. (2010) and Yokoyama et al. (2022) for their calcite standards.

3. Results

3.1. XRD analysis of the experimental products

The XRD pattern of Dol#0 is shown in Fig. 1 together with that of the ACMC after dehydration. The XRD patterns of all the synthetic dolomites and calcite are shown in Fig. S1. These XRD patterns show that the ACMC remained amorphous after dehydration, but it crystallized to dolomite after heating. No other phase can be identified. Note that the XRD analysis was done after washing the synthetic dolomites. Before washing, we identified some impurities such as northupite ($Na_3Mg(CO_3)_2Cl$) and eitelite ($Na_2Mg(CO_3)_2$), all of which dissolved in water and disappeared after washing (Sugawara et al., 2022).

3.2. Chemical compositions of the synthetic dolomites and calcite

Fig. 2 shows the backscattered electron image (BEI) of Dol#0. The BEIs of all the synthetic dolomites and calcite are shown in Fig. S2. We did not identify any impurity and found only dolomite particles, supporting the results of the XRD analysis. Fig. 3 shows the MnO and Cr_2O_3 abundances in the synthetic dolomites and calcite measured using EPMA. We did not find any heterogeneity throughout the sample mount in a scale of electron beam diameter, ~10 μm, which is almost comparable to that of the primary ion beam in the SIMS measurement.

The average chemical compositions of Dol#0, Dol#2, Dol#6, and Cal#0 are summarized in Table 1. The CO_2 abundances were calculated assuming that Na, Mg, Ca, Cr, Mn, and Fe are present as Na_2CO_3, $MgCO_3$, $CaCO_3$, $CrCO_3$, $MnCO_3$, and $FeCO_3$, respectively.

The $^{55}Mn/^{52}Cr$ (mol/mol) ratios are 2.42 ± 0.02 for Dol#0 (2SE, N = 622), 0.618 ± 0.007 for Dol#2 (2SE, N = 199), 1.20 ± 0.02 for Dol#6 (2SE, N = 197), and 0.860 ± 0.011 for Cal#0 (2SE, N = 196). The Fe mol% (in total cations) are 1.88 ± 0.01 for Dol#2 (2SE, N = 199) and 5.80 ± 0.02 (2SE, N = 197) for Dol#6. The synthetic dolomites have higher Ca/Mg ratios than the ideal stoichiometry of 1. The higher Ca/Mg ratios are likely inherited from the Ca/Mg ratios of the starting solutions. Alternatively, the high Ca/Mg ratio may indicate an incomplete crystallization. However, Sugawara et al. (2022) conducted EPMA, XRD, and TG-DTA analyses of ACMC and showed that the longer ACMC is heated, the higher the Ca/Mg ratio of dolomite is. After heating at 360 °C for 12 hours, the Ca/Mg ratio reached plateau. The total abundances of the measured elements in the synthetic dolomites and calcite are lower than 100%, ranging from 83 to 92 wt%. These lower total abundances are attributed to pores in the pellet samples (Fig. 2).

3.3. RSF values of the synthetic dolomites and calcite

We found that the $^{55}Mn^{+}/^{52}Cr^{+}$ ion intensity ratios of synthetic dolomites and calcite decreased during a single analysis by more than 10s of % (Fig. 4). In other words, the RSF values are dependent on time and the depth of SIMS pits. This behavior was also reported by Sugiura et al. (2010) and Jilly et al. (2014) and in sharp contrast to what was observed for San Carlos olivine. The similar time dependency was observed for the Ivuna dolomite analyzed here (Fig. 4) and attests that Cr and Mn are incorporated into dolomite crystals and not into, e.g., grain boundaries, as inferred from the XRD analyses showing no presence of other phases than dolomite (Figs, 1 and S1). Therefore, we used the average intensity ratio calculated from the total $^{55}Mn^{+}$ and $^{52}Cr^{+}$ counts (see section 2.4)

298 to define the RSF value for each measurement of the synthetic dolomites. To avoid the
299 problem of time-dependent RSF values and to use the defined RSF values, we measured
300 the standard and unknown samples in the same sequence and under the same conditions.
301 We summarized the RSF values of the synthetic dolomites and calcite in Fig. 5 and Table
302 2.

303 We found that the synthetic dolomites with higher Fe contents appear to show higher RSF
304 values (Fig. 5). The RSF values of Dol#0, Dol#2, and Dol#6 in days 1-3 are 0.786 ± 0.023
305 (2SD, N = 5), 0.778 ± 0.060 (2SD, N = 10), and 0.820 ± 0.039 (2SD, N = 9), respectively.
306 In day 4, they are 0.824 ± 0.021 (2SD, N = 3), 0.861 ± 0.040 (2SD, N = 3), and 0.884 ±
307 0.047 (2SD, N = 3). The RSF value of Cal#0 is 0.709 ± 0.022 (2SD, N = 5) in days 1-3
308 and 0.719 ± 0.063 (2SD, N = 3) in day 4. The RSF values of Dol#0, Dol#2, and Dol#6 in
309 day 4 are systematically higher than those in days 1-3 (Fig. 5), likely due to a slight change
310 in the detection efficiency of the EMs. Thus, the $^{55}Mn^{+}/^{52}Cr^{+}$ ratios of the Ivuna dolomite
311 in days 1-3 and in day 4 are separately corrected using the RSF values in days 1-3 and in
312 day 4, respectively. The RSF value of Cal#0 is broadly consistent with those of calcite
313 reported by previous studies (e.g., Sugiura et al., 2010; Fujiya et al., 2012; 2013; 2022;
314 Jilly et al., 2014) and slightly smaller than those of Dol#0, Dol#2, and Dol#6. It should
315 be emphasized that the reproducibility of the RSF values is as good as 3-5% for Dol#0,
316 Dol#6, and Cal#0 in days 1-3 even if the $^{55}Mn^{+}/^{52}Cr^{+}$ ratios changed drastically during a
317 single analysis (Fig. 5). For Dol#2, the reproducibility of the RSF values is ~8%, slightly
318 worse than the other synthetic dolomites and calcite, but the reason is unclear. We note
319 that the variation in RSF values between the synthetic dolomites and calcite is most
320 pronounced at the beginning of the measurements, and that their RSF values converged
321 at the end (Fig. 4).

To evaluate the RSF value at a given Fe content and its reproducibility, we drew a regression line of the data in a RSF values (y) vs. Fe contents (x) space and we adopt the 95% confidence interval of the inferred RSF values (Fig. 5). The standard deviation of the RSF value (σ_{RSF}) at a given Fe content, x_0, is given by

$$\sigma_{RSF} = \sqrt{V\left(1 + \frac{1}{n} + \frac{(x_0 - \bar{x})^2}{S_{xx}}\right)}$$

where V is the variance of y residuals, S_{xx} is the summation of x^2, $\bar{x}$ is the average of x, and n is the number of the data. To obtain the 95% confidence interval, we multiplied σ_{RSF} by $t(n-2,0.05)$ from student's t table. We used linear regression for simplicity, as opposed to exponential regression adopted by previous studies (McCain et al., 2020; 2023). However, given the small dependence of the RSF values on Fe contents and relatively poor reproducibility of the data, the difference between linear and exponential regression is negligible. The counting statistics (Poisson error) of $^{55}Mn^+/^{52}Cr^+$ ratios and σ_{RSF} were propagated to the final errors on the $^{55}Mn/^{52}Cr$ ratios of the Ivuna dolomite.

3.4. The Mn-Cr age of dolomite grains in Ivuna

The Fe mol% (in total cations) of the analyzed dolomite grains, Ivuna-H2 dolomite #7 and dolomite #3, range from 2.8 to 3.6 (Table 3). Although Fe contents are much more homogeneous than Mn among individual dolomite grains (Johnson and Prinz, 1993; Endress and Bischoff, 1996; Piralla et al., 2020), we took the zoning of Fe within the analyzed grains into account and measured the Fe contents at each SIMS pit to calculate the corresponding RSF values. The RSF values for Ivuna-H2 dolomite #7 and #3 are from 0.794 to 0.800 (days 1-3) and from 0.864 to 0.865 (day 4), and the 95% confidence

interval of the inferred RSF values is approximately 0.050 (Table 3).

We show the results of the Mn-Cr isotope analysis of Ivuna-H2 dolomite #7 and #3 in Table 3. These data are also displayed in a Mn-Cr isochron diagram (Fig. 6a). The $\delta^{53}Cr$ values of Ivuna-H2 dolomite #7 and #3 are up to ~2,400‰ and correlate with $^{55}Mn/^{52}Cr$ ratios ranging from ~500 to ~60,000. In Fig. 6b, we show the data in a $\delta^{53}Cr$ vs. $1/^{52}Cr$ space and found a much weaker correlation than that in the Mn-Cr isochron diagram. These observations suggest that the correlation in the Mn-Cr isochron diagram results from *in-situ* decay of ^{53}Mn rather than a mixing line. The data obtained in days 1-3 and in day 4 are shown together in Fig. 6a, and both the dataset plot on a single regression line. The $(^{53}Mn/^{55}Mn)_0$ ratio inferred from the slope of the regression line is $(3.95 \pm 0.49) \times 10^{-6}$ (95% confidence interval, MSWD = 0.88). The y-intercept, which corresponds to the initial $\delta^{53}Cr$ value, is 1± 20‰.

4. Discussion

4.1. Comparison between the RSF values in this study and in previous studies

The RSF values of Dol#0, Dol#2, and Dol#6 are 0.786, 0.778, and 0.820 (days 1-3), which are lower than those of Cr-implanted carbonate standards evaluated by previous studies (Steele et al., 2017; McCain et al., 2020; 2023). For example, McCain et al. (2023) reported RSF values of ~1.06, ~1.32, ~1.18, and ~1.39 for dolomites with 0 (below detection limit), ~0.9, ~1.4, and ~8.0 mol% Fe, respectively (Fig. 5). Note that here we define RSF as $(^{55}Mn^+/^{52}Cr^+)_{SIMS}/(^{55}Mn/^{52}Cr)_{true}$, which is the same as that adopted by some previous studies (Sugiura et al., 2010; Fujiya et al., 2012; 2013; 2022; Jilly et al., 2014) but in an inverse definition to what appears in other previous studies (Steele et al.,

2017; McCain et al., 2020; 2023). Thus, the above RSF values obtained by McCain et al. (2023) are corrected according to the definition in this study.

This difference between RSF values in previous studies (Steele et al., 2017; McCain et al., 2020; 2023) and this study may be due to different analytical conditions. The previous studies used a scanning primary ion beam to analyze a large area (e.g., 100 × 100 μm^2) of sample surface to obtain accurate depth profiles (e.g., from the surface to the depth of ~250 nm) of Cr implanted into the shallow layer. On the other hand, this study used a focused primary beam at a small spot producing a deep SIMS pit, which is the same condition for unknown samples.

Sugiura et al. (2010) found that RSF values varied depending on the depth of SIMS pits. They reported that spot (non-scanning) analysis resulted in RSF values decreasing with time (i.e., the depth of SIMS pits) during a single analysis, as observed in this study (Fig. 4). The large (10s of %) change in the RSF values with time shown in Fig. 4 would correspond to the formation of deep SIMS pits due to a high sputtering rate of carbonates. Such a drastic change in observed secondary ion intensity ratios was also reported for other elements in carbonates, e.g., $^{24}Mg/^{42}Ca$, $^{88}Sr/^{42}Ca$, and $^{138}Ba/^{42}Ca$, which is dependent on instruments and tuning conditions (Gabitov et al., 2013). The higher RSF values in the previous studies may be due to the fact that the RSF values were determined from the shallow areas of the Cr-implanted standards. Indeed, the RSF values at the surface shown in Fig. 4 are close to those of the previous studies. Therefore, the previous studies likely obtained higher RSF values than what should actually be used for unknown samples analyzed at small spots (with deep SIMS pits) due to a limited grain size of carbonates. The above argument demonstrates that analytical conditions including

spot/scanning analysis and measurement time must be kept consistent between standard carbonates and unknown samples, which is not achieved by Steele et al. (2017) and McCain et al. (2023).

The RSF values of the synthetic dolomites are dependent on their Fe contents (Fig. 5 and Table 2). These trends have also been reported by previous studies (Steele et al., 2017; McCain et al., 2020; 2023), although the extent of the trends varied among individual studies. The dependence on Fe contents may be attributed to the electric conductivity of the samples, which influences the electric charge state of the sample surface, and as a result, the secondary ion yields (Steele et al., 2017). These observations attest that we must use a dolomite standard with a similar Fe content to unknown samples for Mn-Cr dating of dolomite. We found that the variation in RSF values between the synthetic dolomites is most pronounced at the surface (beginning of the measurements) but is smaller at the end (Fig. 4). Therefore, if we determine RSF values at the surface, the similarly large Fe dependence to that obtained by the previous studies may be observed.

Finally, we mention the complications regarding the RSF values of the synthetic dolomites which should be assessed by future work. First, the Cr contents of the synthetic dolomites are much higher than the natural abundances in dolomite in Ivuna and Ryugu samples, and the influences of Cr on RSF values is unknown. Nevertheless, the Cr contents of our synthetic dolomites are variable by a factor of 4, on the other hand, the variability in their RSF values is only ~5% (in days 1-3) and ~7% (in day 4). Thus, the Cr abundance of dolomite seems to have little impact on its RSF value. Second, the Ca/Mg (mol/mol) ratios of the synthetic dolomites deviate from ideal stoichiometry (= 1), ranging from 1.39 to 1.53, which are also higher than those observed for the Ivuna

dolomites ranging from 1.06 to 1.16. Calcium and Mg abundances could also affect matrix effect. Based on the results of Steele et al. (2017), however, the RSF values of ankerite (MgO ~ 17 wt%), dolomite (MgO ~ 33 wt%), and magnesite (MgO ~ 95 wt%) are similar, ranging from 0.69 to 0.81. Thus, we expect that Ca/Mg ratios do not have a large impact on RSF values, and it is hard to see to what extent the relationship between RSF values and Ca and Mg abundances is due to the variation in Fe contents.

4.2. The $(^{53}Mn/^{55}Mn)_0$ ratio of Ivuna dolomite and update on the age of Ryugu carbonates

Our new $(^{53}Mn/^{55}Mn)_0$ of the Ivuna dolomite is $(3.95 \pm 0.49) \times 10^{-6}$, which is 26 ± 19% higher than that obtained by Yokoyama et al. (2023a) using a calcite standard, i.e., $(3.14 \pm 0.28) \times 10^{-6}$, for the same grain. In this study, we used RSF values from 0.794 to 0.865 depending on Fe contents of the analyzed dolomites and analysis dates, which are ~12% (day 1-3) or ~20% (day 4) higher than that of Cal#0. Thus, we concluded that the $(^{53}Mn/^{55}Mn)_0$ difference between Yokoyama et al. (2023a) and this study resulted from the RSF difference between calcite and dolomite.

We note that the pellet samples of our synthetic dolomites are porous (Figs. 2 and S2), on the other hand, typical dolomites in Ivuna and Ryugu are not (Yokoyama et al., 2023a; McCain et al., 2023), which could result in different sputtering behavior of SIMS and affect RSF values. However, the changes in the observed $^{55}Mn^+/^{52}Cr^+$ ratios are similar between the synthetic and Ivuna dolomites (Fig. 4). Moreover, Yokoyama et al. (2023a), who also used a pellet sample of calcite as a standard, and this study obtained a similar RSF value of calcite to that obtained by Sugiura et al. (2010) who analyzed larger crystals of a synthetic calcite than that we produced in this study. These observations suggest that

porosity seems to have little impact on RSF values.

Based on the results of the Ivuna dolomite, we try updating the $(^{53}Mn/^{55}Mn)_0$ ratio of $(2.55 \pm 0.35) \times 10^{-6}$ for dolomite in Ryugu A0058 reported by Yokoyama et al. (2023a), because they were analyzed under the same conditions. Using the 26 ± 19% difference between Yokoyama et al. (2023a) and this study, we corrected the $(^{53}Mn/^{55}Mn)_0$ ratio of the Ryugu A0058 dolomite to be $(3.21 \pm 0.66) \times 10^{-6}$. The attached error was evaluated by propagating the errors on the $(^{53}Mn/^{55}Mn)_0$ ratios used for the calculation.

The $(^{53}Mn/^{55}Mn)_0$ ratio of $(3.95 \pm 0.49) \times 10^{-6}$ for the Ivuna dolomite can be converted to an absolute age of 4564.0 +0.6/−0.7 Ma using a quenched angrite D'Orbigny as a time anchor with a known $(^{53}Mn/^{55}Mn)_0$ of 3.54×10^{-6} (McKibbin et al., 2015) and Pb-Pb age of 4563.37 Ma (Brennecka and Wadhwa, 2012). Similarly, the $(^{53}Mn/^{55}Mn)_0$ ratio of $(3.21 \pm 0.66) \times 10^{-6}$ for the Ryugu A0058 dolomite corresponds to an absolute age of 4562.8 +1.0/−1.2 Ma. This age is our best estimate for the formation time of dolomite in Ryugu, although there is no guarantee that all the dolomite grains in Ryugu formed at the same time.

In the following, we discuss the $(^{53}Mn/^{55}Mn)_0$ ratios of Ryugu carbonates reported by previous studies. We note that, however, RSF values are sensitive to the analytical conditions and instrument, and thus, simple comparison of $(^{53}Mn/^{55}Mn)_0$ ratios based on the RSF values used is difficult. Thus, we could provide only a qualitative discussion below in contrast to the correction for the Ryugu A0058 dolomite which are based on the difference between the $(^{53}Mn/^{55}Mn)_0$ ratios (not between RSF values) obtained by Yokoyama et al. (2023a) and this study.

Nakamura et al. (2022) reported a $(^{53}Mn/^{55}Mn)_0$ ratio of $(4.14 \pm 0.68) \times 10^{-6}$, which is

consistent with our new $(^{53}Mn/^{55}Mn)_0$ of the Ivuna dolomite. Nakamura et al. (2022) used a synthetic calcite standard, but the RSF value used is 0.829, substantially higher than that of Cal#0 and rather close to those of our synthetic dolomites. Therefore, if the RSF value of dolomite is slightly higher than that of calcite, as inferred from this study, then their $(^{53}Mn/^{55}Mn)_0$ will be higher than the original value obtained by Nakamura et al. (2022).

On the other hand, McCain et al. (2023) obtained much higher $(^{53}Mn/^{55}Mn)_0$ of $(6.8 \pm 0.5) \times 10^{-6}$ and $(6.1 \pm 0.9) \times 10^{-6}$ for dolomite in Ryugu A0037 and for combined dolomite (dominant), breunnerite, and Ca-carbonate in Ryugu C0009, respectively, than our $(^{53}Mn/^{55}Mn)_0$ of the Ivuna dolomite. They used a higher RSF value of 1.25 than our values for the Ivuna dolomite grains analyzed. As discussed above, their elevated RSF value is likely attributed to the shallower SIMS pits produced by scanning analysis on large areas (50×50 μm^2) of the standards than those on the Ryugu carbonates. Therefore, the RSF value to be used for Ryugu carbonates appears lower than 1.25, and the reported $(^{53}Mn/^{55}Mn)_0$ ratios are likely too high. Because the difference between RSF values used by McCain et al. (2023) and this study results in a lower $(^{53}Mn/^{55}Mn)_0$ by a factor of ~1.6 (corresponding to an age shift of ~2.4 Myr), if the $(^{53}Mn/^{55}Mn)_0$ of McCain et al (2023) is corrected using the RSF in this study, the $(^{53}Mn/^{55}Mn)_0$ of McCain et al (2023) will be consistent with the $(^{53}Mn/^{55}Mn)_0$ of the Ivuna dolomite in this study.

4.3. Implications from the Mn-Cr ages of CI and Ryugu dolomites for aqueous alteration in their parent bodies

Based on the newly determined RSF values, our best estimates for the $(^{53}Mn/^{55}Mn)_0$ ratios

of Ivuna and Ryugu dolomite are (3.95 ± 0.49) × 10^{-6} and (3.21 ± 0.66) × 10^{-6}, respectively, which correspond to the formation ages of 4564.0 +0.6/−0.7 Ma and 4562.8 +1.0/−1.2 Ma. These $(^{53}Mn/^{55}Mn)_0$ ratios are close to the values of (2.6 ± 0.7) × 10^{-6} and (3.12 ± 0.34) × 10^{-6} estimated for whole-rock Ryugu samples (Yokoyama et al., 2023b; Tanaka et al., 2024). The variation in $^{55}Mn/^{52}Cr$ and $^{53}Cr/^{52}Cr$ ratios between the whole-rock samples seems to reflect heterogeneity in samples of small mass, and thus, their $^{55}Mn/^{52}Cr$ and $^{53}Cr/^{52}Cr$ ratios would be controlled by the distribution of carbonates. If true, the whole-rock $(^{53}Mn/^{55}Mn)_0$ ratios would record the timing of carbonate formation.

Previous studies (e.g., Fujiya et al., 2013; McCain et al., 2023) have put the ages of carbonate into the context of the accretion time of the CI/Ryugu parent bodies. Our age of the Ivuna dolomites is older than the previously reported ages of CI dolomites by 0.2-1.5 Myr (Fujiya et al., 2013). Therefore, the accretion age (3-4 Myr after CAIs) estimated from a thermal modelling will be older accordingly, resulting in higher peak temperature in the CI parent body associated with a higher amount of ^{26}Al as a heat source. It should be noted, however, that the peak temperature estimated is highly dependent on the model settings such as water ice abundance, the reaction heat of hydration, and water circulation in the parent body. McCain et al. (2023) argued an early accretion of the Ryugu parent body within 1.8 Myr after CAIs based on their carbonate ages, which requires a small size or early disruption for the Ryugu parent body to reconcile the early accretion age with the low temperatures inferred for Ryugu samples (up to 80 °C based on oxygen isotope thermometry; Nakamura et al., 2022; Yokoyama et al., 2023a; McCain et al., 2023; Kita et al., 2024). The age of the Ryugu dolomites updated here relaxes this temperature constraint, and the early accretion/disruption of a small planetesimal is no longer necessary.

Interestingly, our new ages are close to the ^{129}I-^{129}Xe age of 4564.3 ± 0.3 Ma for magnetite separated from Orgueil (Pravdivtseva et al., 2018). Magnetite in CI and Ryugu samples has a wide range of O isotopic compositions recording the change in the temperatures and compositions of aqueous fluids during progressive alteration (Rowe et al., 1994; Nakamura et al., 2022; Yokoyama et al., 2023a; McCain et al., 2023; Fujiya et al., 2023; Kita et al., 2024). On the other hand, the O isotopic compositions of dolomite are relatively homogeneous, indicating its formation when the system was approaching equilibrium (Piralla et al., 2020; Nakamura et al., 2022; Yokoyama et al., 2023a; McCain et al., 2023; Fujiya et al., 2023; Kita et al., 2024). These observations on the formation ages and O isotopic compositions of dolomite and magnetite suggest that the aqueous alteration progressed quickly in a timescale of Myr. Note that Ca-carbonate in CI and Ryugu samples tend to have O isotopic compositions suggesting its earlier formation than dolomite (McCain et al., 2023; Fujiya et al., 2023). Therefore, the Mn-Cr age of Ca-carbonate could be older than that of dolomite and shed light on the alteration period of CI and Ryugu parent bodies, although the Mn-Cr dating might be difficult due to low Mn abundances of Ca-carbonate compared to dolomite (Endress and Bischoff, 1996; Piralla et al., 2020).

5. Conclusions

We aim at improving the accuracy of Mn-Cr dating of dolomite in carbonaceous chondrites and assessing apparently inconsistent Mn-Cr ages previously reported. For this purpose, we synthesized Mn-, Cr-, and Fe-bearing dolomite standards and evaluated their Mn/Cr RSF values for SIMS (here defined by $(^{55}Mn^{+}/^{52}Cr^{+})_{SIMS}/(^{55}Mn/^{52}Cr)_{true}$). We

found that (i) the RSF values of dolomites range from 0.8 to 0.9, higher than that of calcite (~0.7), that (ii) the RSF values decreased by 10s of % during a single analysis with a SIMS pit deepening, and that (iii) the RSF values are dependent on the Fe contents in dolomite. All the three findings above point to the importance of using a proper, matrix-matched dolomite standard as well as of analyzing the standard and unknown samples under consistent conditions (e.g., primary beam current, measurement time, and spot/scanning analysis). Previously reported RSF values much higher than our new results are attributed to the difference between the SIMS pits resulting from different analytical conditions (scanning analysis on a large surface area in previous studies and spot analysis on a small region in this study). Therefore, measurements combining different analytical conditions between standards and unknown samples will result in erroneous Mn-Cr ages. This argument explains why some of the previous Mn-Cr ages of Ryugu dolomite are extremely old. We emphasize that the new synthetic dolomite standards with homogeneous Cr contents enabled us to analyze the standards and unknown samples under consistent conditions and correct $^{55}Mn/^{52}Cr$ ratios using appropriate RSF values.

Using our new RSF values, we obtained a $(^{53}Mn/^{55}Mn)_0$ ratio of $(3.95 \pm 0.49) \times 10^{-6}$ (95% confidential interval) and the corresponding absolute age of 4564.0 +0.6/−0.7 Ma for Ivuna dolomite. We also updated the $(^{53}Mn/^{55}Mn)_0$ ratio previously reported for dolomite in the Ryugu sample A0058 to be $(3.21 \pm 0.66) \times 10^{-6}$, which corresponds to an absolute age of 4562.8 +1.0/−1.2 Ma. This age is our best estimate for the formation age of dolomite in Ryugu. Taking our Mn-Cr ages of CI/Ryugu dolomite and the I-Xe age of CI magnetite together, we conclude that aqueous alteration in CI and Ryugu parent bodies progressed quickly, likely in a timescale of Myr.

Acknowledgements

The Ivuna specimen used in this study was kindly proved by Dr. Sara S. Russell (Natural History Museum, UK). This work was supported by JSPS KAKENHI Grant Numbers 22K18722 (N.K.), 22H01279 (W.F.), and 23H00146 (W.F.). This work was supported by ISSI in Bern and Beijing, through the International Team project "Timing and Processes of Planetesimal Formation and Evolution".

Data Availability

Data are available through Zenodo at https://doi.org/ 10.5281/zenodo.10963183.

Appendix A. Supplementary material

Appendix A. includes the XRD patterns (Fig. S1) and BEIs (Fig. S2) of all the synthetic dolomites and calcite.

References

Alexander, C.M.O'D., Bowden, R., Fogel, M.L., Howard, K.T., Herd, C.D.K., Nittler, L.R., 2012. The provenances of asteroids, and their contributions to the volatile inventories of the terrestrial planets. Science 337, 721−723.

Brearley, A.J., 2006. The action of water. in: Lauretta, D.S., McSween, H.Y.Jr. (Eds.), Meteorites and the Early Solar System II, University of Arizona Press, Tucson, pp. 587−624.

Brennecka, G.A., Wadhwa, M., 2012. Uranium isotope compositions of the basaltic angrite meteorites and the chronological implications for the early Solar System. Proc. Natl. Acd. Sci. 109, 9299−9303.

Bullock, E.S., Gounelle, M., Lauretta, D.S., Grady, M.M., Russell, S.S., 2005. Mineralogy and texture of Fe-Ni sulfides in CI1 chondrites: Clues to the extent of aqueous alteration on the CI1 parent body. Geochim. Cosmochim. Acta 69, 2687−2700.

Cohen, B.A., Coker, R.F., 2000. Modeling of liquid water on CM meteorite parent bodies and implications for amino acid racemization. Icarus 145, 369−381.

Doyle, P.M., Jogo, K., Nagashima, K., Krot, A.N., Wakita, S., Ciesla, F.J., Hutcheon, I.D., 2015. Early aqueous activity on the ordinary and carbonaceous chondrite parent bodies recorded by fayalite. Nat. Commun. 6:7444.

Endress, M., Bischoff, A., 1996. Carbonates in CI chondrites: Clues to parent body evolution. Geochim. Cosmochim. Acta 60, 489−507.

Endress, M., Zinner, E., Bischoff, A., 1996. Early aqueous activity on primitive meteorite

589 parent bodies. Nature 379, 701−703.

590 Fujiya, W., Sugiura, N., Hotta, H., Ichimura, K., Sano, Y., 2012. Evidence for the late
591 formation of hydrous asteroids from young meteoritic carbonates. Nat. Commun.
592 3:627.

593 Fujiya, W., Sugiura, N., Sano, Y. Hiyagon, H., 2013. Mn–Cr ages of dolomites in CI
594 chondrites and the Tagish Lake ungrouped carbonaceous chondrite. Earth Planet. Sci.
595 Lett. 362, 130−142.

596 Fujiya, W., Higashi, H., Hibiya, Y., Sugawara, S., Yamaguchi, A., Kimura, M.,
597 Hashizume, K. 2022. Hydrothermal activities on C-complex asteroids induced by
598 radioactivity. Astrophys. J. Lett. 924:L16 (10pp).

599 Fujiya, W., Kawasaki, N., Nagashima, K., Sakamoto, N., Alexander, C.M.O'D., Kita,
600 N.T., Kitajima, K., Abe, Y., Aléon, J., Amari, S., Amelin, Y., Bajo, K., Bizzarro, M.,
601 Bouvier, A., Carlson, R.W., Chaussidon, M., Choi, B.-G., Dauphas, N., Davis, A.M.,
602 Di Rocco, T., Fukai, R., Gautam, I., Haba, M.K., Hibiya, Y., Hidaka, H., Homma, H.,
603 Hoppe, P., Huss, G.R., Ichida, K., Iizuka, T., Ireland, T.R., Ishikawa, A., Itoh, S.,
604 Kleine, T., Komatani, S., Krot, A.N., Liu, M.-C., Masuda, Y., McKeegan, K.D.,
605 Morita, M., Motomura, K., Moynier, F., Nakai, I., Nguyen, A., Nittler, L.R., Onose,
606 M., Pack, A., Park, C., Piani, L., Qin, L., Russell, S.S., Schönbächler, M., Tafla, L.,
607 Tang, H., Terada, K., Terada, Y., Usui, T., Wada, S., Wadhwa, M., Walker, R.J.,
608 Yamashita, K., Yin, Q.-Z., Yokoyama, T., Yoneda, S., Young, E.D., Yui, H., Zhang,
609 A.-C., Nakamura, T., Naraoka, H., Noguchi, T., Okazaki, R., Sakamoto, K., Yabuta,
610 H., Abe, M., Miyazaki, A., Nakato, A., Nishimura, M., Okada, T., Yada, T., Yogata,
611 K., Nakazawa, S., Saiki, T., Tanaka, S., Terui, F., Tsuda, Y., Watanabe, S., Yoshikawa,

612 M., Tachibana, S., Yurimoto, H., 2023. Carbonate record of temporal change in
613 oxygen fugacity and gaseous species in asteroid Ryugu. Nat. Geosci. 16, 675−682.

614 Gabitov, R.I., Gagnon, A.C., Guan, Y., Eiler, J.M., Adkins, J.F., 2013. Accurate Mg/Ca,
615 Sr/Ca, and Ba/Ca ratio measurements in carbonates by SIMS and NanoSIMS and an
616 assessment of heterogeneity in common calcium carbonate standards. Chem. Geol.
617 356, 95−108.

618 Grady, M.M., Wright, I.P., 2003. Elemental and isotopic abundances of carbon and
619 nitrogen in meteorites. Space Sci. Rev. 106, 231−248.

620 Grimm, R.E., McSween, H.Y.Jr., 1989. Water and the thermal evolution of carbonaceous
621 chondrite parent bodies. Icarus 82, 244−280.

622 Holland, H.D., Zimmermann, H., 2000. The dolomite problem revisited. Int. Geol. Rev.
623 42, 481−490.

624 Hoppe, P., MacDougall, D., Lugmair, G.W., 2007. High spatial resolution ion microprobe
625 measurements refine chronology of carbonate formation in Orgueil. Meteorit. Planet.
626 Sci. 42, 1309−1320.

627 Hua, X., Buseck, P.R., 1998. Unusual forms of magnetite in the Orgueil carbonaceous
628 chondrite. Meteorit. Planet. Sci. 33, A215−A220.

629 Jilly, C.E., Huss, G.R., Krot, A.N., Nagashima, K., Yin, Q.-Z., Sugiura, N., 2014. ^{53}Mn-
630 ^{53}Cr dating of aqueously formed carbonates in the CM2 lithology of the Sutter's Mill
631 carbonaceous chondrite. Meteorit. Planet. Sci. 49, 2104−2117.

632 Johnson, C.A., Prinz, M. 1993. Carbonate compositions in CM and CI chondrites, and
633 implications for aqueous alteration. Geochim. Cosmochim. Acta 57, 2843−2852.

King, A.J., Schofield, P.E., Howard, K.T., Russell, S.S., 2005. Modal mineralogy of CI and CI-like chondrites by X-ray diffraction. Geochim. Cosmochim. Acta 165, 148−160.

Kita, N.T., Kitajima K., Nagashima, K., Kawasaki, N., Sakamoto, N., Fujiya, W., Abe, Y., Aléon, J., Alexander, C.M.O'D., Amari, S., Amelin, Y., Bajo, K., Bizzarro, M., Bouvier, A., Carlson, R.W., Chaussidon, M., Choi, B.-G., Dauphas, N., Davis, A.M., Di Rocco, T., Fukai, R., Gautam, I., Haba, M.K., Hibiya, Y., Hidaka, H., Homma, H., Hoppe, P., Huss, G.R., Ichida, K., Iizuka, T., Ireland, T.R., Ishikawa, A., Itoh, S., Kleine, T., Komatani, S., Krot, A.N., Liu, M.-C., Masuda, Y., McKeegan, K.D., Morita, M., Motomura, K., Moynier, F., Nakai, I., Nguyen, A., Nittler, L.R., Onose, M., Pack, A., Park, C., Piani, L., Qin, L., Russell, S.S., Schönbächler, M., Tafla, L., Tang, H., Terada, K., Terada, Y., Usui, T., Wada, S., Wadhwa, M., Walker, R.J., Yamashita, K., Yin, Q.-Z., Yokoyama, T., Yoneda, S., Young, E.D., Yui, H., Zhang, A.-C., Nakamura, T., Naraoka, H., Noguchi, T., Okazaki, R., Sakamoto, K., Yabuta, H., Abe, M., Miyazaki, A., Nakato, A., Nishimura, M., Okada, T., Yada, T., Yogata, K., Nakazawa, S., Saiki, T., Tanaka, S., Terui, F., Tsuda, Y., Watanabe, S., Yoshikawa, M., Tachibana, S., Yurimoto, H., 2024. Disequilibrium oxygen isotope distribution among aqueously altered minerals in Ryugu asteroid returned samples. Meteorit. Planet. Sci. 59, 2097−2116.

Krot, A.N., Nagashima, K., Alexander, C.M.O'D., Ciesla, F.J., Fujiya, W., Bonal, L., 2015. Sources of water and aqueous activity on the chondrite parent asteroids. in: Michel, P., DeMeo, F.E., Bottke, W.F. (Eds.), Asteroids IV, University of Arizona Press, Tucson, pp. 635−660.

657 Land, L.S., 1998. Failure to precipitate dolomite at 25 ℃ from dilute solution despite
658 1000-fold oversaturation after 32 years. Aquat. Geochem. 4, 361−368.

659 Macdougall, J.D., Lugmair, G.W., 1984. Early Solar System aqueous activity: Sr isotope
660 evidence from the Orgueil CI chondrite. Nature 307, 249−251.

661 McCain, K.A., Liu, M.-C., McKeegan, K.D., 2020. Calibration of matrix-dependent
662 biases in isotope and trace element analyses of carbonate minerals. J. Vac. Sci. Technol.
663 B 38, 044005.

664 McCain, K.A., Matsuda, N., Liu, M.-C., McKeegan, K.D., Yamaguchi, A., Kimura, M.,
665 Tomioka, N., Ito, M., Imae, N., Uesugi, M., Shirai, N., Ohigashi, T., Greenwood, R.C.,
666 Uesugi, K., Nakato, A., Yogata, K., Yuzawa, H., Kodama, Y., Hirahara, K., Sakurai,
667 I., Okada, I., Karouji, Y., Nakazawa, S., Okada, T., Saiki, T., Tanaka, S., Terui, F.,
668 Yoshikawa, M., Miyazaki, A., Nishimura, M., Yada, T., Abe, M., Usui ,T., Watanabe,
669 S., Tsuda, Y., 2023. Early fluid activity on Ryugu inferred by isotopic analyses of
670 carbonates and magnetite. Nat. Astron. 7, 309−317.

671 McKibbin, S.J., Ireland, T.R., Amelin, Y., Holden, P., 2015. Mn−Cr dating of Fe- and
672 Ca-rich olivine from ‘quenched’ and ‘plutonic’ angrite meteorites using Secondary Ion
673 Mass Spectrometry. Geochim. Cosmochim. Acta 157, 13−27.

674 Miyajima, Y., Saito, A., Kagi, H., Yokoyama, T., Takahashi, Y., Hirata, T., 2020.
675 Incorporation of U, Pb and rare earth elements in calcite through crystallisation from
676 amorphous calcium carbonate: Simple preparation of reference materials for
677 microanalysis. Geostand. Geoanalytical Res. 45, 189−205.

678 Montes-Hernandez, G., Renard, F., Auzende, A.-L., Findling, N., 2020. Amorphous

679 calcium-magnesium carbonate (ACMC) accelerates dolomitization at room
680 temperature under abiotic conditions. Cryst. Growth Des. 20, 1434−1441.

681 Nakamura, E., Kobayashi, K., Tanaka, R., Kunihiro, T., Kitagawa, H., Potiszil, C., Ota,
682 T., Sakaguchi, C., Yamanaka, M., Ratnayake, D.M., Tripathi, H., Kumar, R.,
683 Avramescu, M.L., Tsuchida, H., Yachi, Y., Miura, H., Abe, M., Fukai, R., Furuya, S.,
684 Hatakeda, K., Hayashi, T., Hitomi, Y., Kumagai, K., Miyazaki, A., Nakato, A.,
685 Nishimura, M., Okada, T., Soejima, H., Sugita, S., Suzuki, A., Usui, T., Yada, T.,
686 Yamamoto, D., Yogata, K., Yoshitake, M., Arakawa, M., Fujii, A., Hayakawa, M.,
687 Hirata, N., Hirata, N., Honda, R., Honda, C., Hosoda, S., Iijima, Y.I., Ikeda, H.,
688 Ishiguro, M., Ishihara, Y., Iwata, T., Kawahara, K., Kikuchi, S., Kitazato, K.,
689 Matsumoto, K., Matsuoka, M., Michikami, T., Mimasu, Y., Miura, A., Morota, T.,
690 Nakazawa, S., Namiki, N., Noda, H., Noguchi, R., Ogawa, N., Ogawa, K., Okamoto,
691 C., Ono, G., Ozaki, M., Saiki, T., Sakatani, N., Sawada, H., Senshu, H., Shimaki, Y.,
692 Shirai, K., Takei, Y., Takeuchi, H., Tanaka, S., Tatsumi, E., Terui, F., Tsukizaki, R.,
693 Wada, K., Yamada, M., Yamada, T., Yamamoto, Y., Yano, H., Yokota, Y., Yoshihara,
694 K., Yoshikawa, M., Yoshikawa, K., Fujimoto, M., Watanabe, S., Tsuda, Y., 2022. On
695 the origin and evolution of the asteroid Ryugu: A comprehensive geochemical
696 perspective. Proc. Jpn. Acad. Ser. B Phys. Biol. Sci. 98, 227−282.

697 Ogliore, R.C., Huss, G.R., Nagashima, K., 2011. Ratio estimation in SIMS analysis. Nucl.
698 Instrum. Methods Phys. Res. B 269, 1910−1918.

699 Papanastassiou, D.A., 1986. Chromium isotopic anomalies in the Allende meteorite.
700 Astrophys. J. 308, L27−L30.

701 Pina, C.M., Pimentel, C., Crespo, Á., 2020. Dolomite cation order in the geological record.

Chem. Geol. 547, 119667.

Piralla, M., Marrocchi, Y., Verdier-Paoletti, M.J., Vacher, L.G., Villeneuve, J., Piani, L., Bekaert, D.V., Gounelle, M., 2020. Primordial water and dust of the Solar System: Insights from *in situ* oxygen measurements of CI chondrites. Geochim. Cosmochim. Acta 269, 451−464.

Pravdivtseva, O., Krot, A.N., Hohenberg, C.M., 2018. I-Xe dating of aqueous alteration in the CI chondrite Orgueil: I. Magnetite and ferromagnetic separates. Geochim. Cosmochim. Acta 227, 38−47.

Purgstaller, B., Goetschl. K.E., Mavromatis, V., Dietzel, M., 2019. Solubility investigations in the amorphous calcium magnesium carbonate system. CrystEngComm 21, 155−164.

Radha, A.V., Fernandez-Martinez, A., Hu, Y., Jun, Y.-S., Waychunas, G.A., Navrotsky, A., 2012. Energetic and structural studies of amorphous $Ca_{1-x}Mg_xCO_3 \cdot nH_2O$ ($0 \leq x \leq 1$). Geochim. Cosmochim. Acta 90, 83−95.

Rowe, M.W., Clayton, R.N., Mayeda, T.K., 1994. Oxygen isotopes in separated components of CI and CM meteorites. Geochim. Cosmochim. Acta 58, 5341−5347.

Saito, A., Kagi, H., Marugata, S., Komatsu, K., Enomoto, D., Maruyama, K., Kawano, J., 2020. Minerals 10, 270.

Schrader, D.L., Davidson, J., McCoy, T.J., Zega, T.J., Russell, S.S., Domanik, K.J., King, A.J., 2021. The Fe/S ratio of pyrrhotite group sulfides in chondrites: An indicator of oxidation and implications for return samples from asteroids Ryugu and Bennu. Geochim. Cosmochim. Acta 303, 66−91.

724 Steele, R.C.J., Heber, V.S., McKeegan, K.D., 2017. Matrix effects on the relative
725 sensitivity factors for manganese and chromium during ion microprobe analysis of
726 carbonate: Implications for early Solar System chronology. Geochim. Cosmochim.
727 Acta 201, 245−259.

728 Sugawara, S., Fujiya, W., Kagi, H., Yamaguchi, A., Hashizume, K., 2022. Heat-induced
729 dolomitization of amorphous calcium magnesium carbonate in a CO_2-filled closed
730 system. ACS Omega 7, 44670−44676.

731 Sugiura, N., Ichimura, K., Fujiya, W., Takahata, N., 2010. Mn/Cr relative sensitivity
732 factors for synthetic calcium carbonate measured with a NanoSIMS ion microprobe.
733 Geochem. J. 44, e11−e16.

734 Tanaka, R., Ratnayake, D.M., Ota, T., Miklusicak, N., Kunihiro, T., Potiszil, C.,
735 Sakaguchi, C., Kobayashi, K., Kitagawa, H., Yamanaka, M., Abe, M., Miyazaki, A.,
736 Nakato, A., Nakazawa, S., Nishimura, M., Okada, T., Saiki, T., Tanaka, S., Terui, F.,
737 Tsuda, Y., Usui, T., Watanabe, S., Yada, T., Yogata, K., Yoshikawa, M., Nakamura,
738 E., 2024. Unraveling the Cr isotopes of Ryugu: An accurate aqueous alteration age and
739 the least thermally processed solar system material. Astrophys. J. 965:52(11pp).

740 Tomeoka, K., Buseck, P.R., 1988. Matrix mineralogy of the Orgueil CI carbonaceous
741 chondrite. Geochim. Cosmochim. Acta 52, 1627−1640.

742 Visser, R., John, T., Whitehouse, M.J., Patzek, M., Bischoff, A., 2020. A short-lived ^{26}Al
743 induced hydrothermal alteration event in the outer solar system: Constraints from
744 Mn/Cr ages of carbonates. Earth Planet. Sci. Lett. 547, 116440.

745 Warren, J., 2000. Dolomite: occurrence, evolution and economically important

746 associations. Earth-Sci. Rev. 52, 1−81.

747 Weisberg, M.K., McCoy, T.J., Krot, A.N., 2006. Systematic and evaluation of meteorite
748 classification. in: Lauretta, D.S., McSween, H.Y.Jr. (Eds.), Meteorites and the Early
749 Solar System II, University of Arizona Press, Tucson, pp. 19−52.

750 Yokoyama, T., Nagashima, K., Nakai, I., Young, E.D., Abe, Y., Aléon, J., Alexander,
751 C.M.O'D., Amari, S., Amelin, Y., Bajo, K., Bizzarro, M., Bouvier, A., Carlson, R.W.,
752 Chaussidon, M., Choi, B.-G., Dauphas, N., Davis, A.M., Di Rocco, T., Fujiya, W.,
753 Fukai, R., Gautam, I., Haba, M.K., Hibiya, Y., Hidaka, H., Homma, H., Hoppe, P.,
754 Huss, G.R., Ichida, K., Iizuka, T., Ireland, T.R., Ishikawa, A., Ito, M., Itoh, S.,
755 Kawasaki, N., Kita, N.T., Kitajima, K., Kleine, T., Komatani, S., Krot, A.N., Liu, M.-
756 C., Masuda, Y., McKeegan, K.D., Morita, M., Motomura, K., Moynier, F., Nguyen,
757 A., Nittler, L., Onose, M., Pack, A., Park, C., Piani, L., Qin, L., Russell, S.S., Sakamoto,
758 N., Schönbächler, M., Tafla, L., Tang, H., Terada, K., Terada, Y., Usui, T., Wada, S.,
759 Wadhwa, M., Walker, R.J., Yamashita, K., Yin, Q.-Z., Yoneda, S., Yui, H., Zhang,
760 A.C., Connolly, H.C., Jr., Lauretta, D.S., Nakamura, T., Naraoka, H., Noguchi, T.,
761 Okazaki, R., Sakamoto, K., Yabuta, H., Abe, M., Arakawa, M., Fujii, A., Hayakawa,
762 M., Hirata, N., Hirata, N., Honda, R., Honda, C., Hosoda, S., Iijima, Y.I., Ikeda, H.,
763 Ishiguro, M., Ishihara, Y., Iwata, T., Kawahara, K., Kikuchi, S., Kitazato, K.,
764 Matsumoto, K., Matsuoka, M., Michikami, T., Mimasu, Y., Miura, A., Morota, T.,
765 Nakazawa, S., Namiki, N., Noda, H., Noguchi, R., Ogawa, N., Ogawa, K., Okada, T.,
766 Okamoto, C., Ono, G., Ozaki, M., Saiki, T., Sakatani, N., Sawada, H., Senshu, H.,
767 Shimaki, Y., Shirai, K., Sugita, S., Takei, Y., Takeuchi, H., Tanaka, S., Tatsumi, E.,
768 Terui, F., Tsuda, Y., Tsukizaki, R., Wada, K., Watanabe, S., Yamada, M., Yamada, T.,

769 Yamamoto, Y., Yano, H., Yokota, Y., Yoshihara, K., Yoshikawa, M., Yoshikawa, K.,
770 Furuya, S., Hatakeda, K., Hayashi, T., Hitomi, Y., Kumagai, K., Miyazaki, A., Nakato,
771 A., Nishimura, M., Soejima, H., Suzuki, A., Yada, T., Yamamoto, D., Yogata, K.,
772 Yoshitake, M., Tachibana, S., Yurimoto, H., 2023a. Samples returned from the
773 asteroid Ryugu are similar to Ivuna-type carbonaceous meteorites. Science, eabn7850.

774 Yokoyama, T., Wadhwa, M., Iizuka, T., Rai, V., Gautam, I., Hibiya, Y., Masuda, Y.,
775 Haba, M.K., Fukai, R., Hines, R., Phelan, N., Young, E.D., Abe, Y., Aléon, J.,
776 Alexander, C.M.O'D., Amari, S., Amelin, Y., Bajo, K., Bizzarro, M., Bouvier, A.,
777 Carlson, R.W., Chaussidon, M., Choi, B.-G., Dauphas, N., Davis, A.M., Di Rocco, T.,
778 Fujiya, W., Hidaka, H., Homma, H., Hoppe, P., Huss, G.R., Ichida, K., Ireland, T.,
779 Ishikawa, A., Itoh, S., Kawasaki, N., Kita, N.T., Kitajima, K., Kleine, T., Komatani,
780 S., Krot, A.N., Liu, M.-C., McKeegan, K.D., Morita, M., Motomura, K., Moynier, F.,
781 Nakai, I., Nagashima, K., Nguyen, A., Nittler, L., Onose, M., Pack, A., Park, C., Piani,
782 L., Qin, L., Russell, S., Sakamoto, N., Schönbächler, M., Tafla, L., Tang, H., Terada,
783 K., Terada, Y., Usui, T., Wada, S., Walker, R.J., Yamashita, K., Yin, Q.-Z., Yoneda,
784 Young, E.D., S., Yui, H., Zhang, A.-C., Nakamura, T., Naraoka, H., Noguchi, T.,
785 Okazaki, R., Sakamoto, K., Yabuta, H., Abe, M., Miyazaki, A., Nakato, A., Nishimura,
786 M., Okada, T., Yada, T., Yogata, K., Nakazawa, S., Saiki, T., Tanaka, S., Terui, F.,
787 Tsuda, Y., Watanabe, S., Yoshikawa, M., Tachibana, S., Yurimoto, H., 2023b. Water
788 circulation in Ryugu asteroid affected the distribution of nucleosynthetic isotope
789 anomalies in returned sample. Sci. Adv. 9, eadi7048.

790 Zolensky, M., Barrett, R., Browning, L., 1993. Mineralogy and compositions of matrix
791 and chondrule rims in carbonaceous chondrites. Geochim. Cosmochim. Acta 57,

792 3123−3148.

Table 1

Chemical compositions of synthetic dolomites and calcite.

Sample	Na_2O (wt%)	MgO (wt%)	MnO (wt%)	CaO (wt%)	FeO (wt%)	Cr_2O_3 (wt%)	Cl (wt%)	CO_2 (wt%)	Total (wt%)	*N*	Fe (mol%) *	2SE	$^{55}Mn/^{52}Cr$ (mol/mol)	2SE
Cal#0	0.25	b.d.	0.72	49.43	b.d.	1.06	0.07	40.03	91.58	196	b.d.	-	0.860	0.011
Dol#0	0.22	14.57	0.64	28.08	b.d.	0.34	0.13	38.70	82.69	622	b.d.	-	2.42	0.02
Dol#2	0.20	13.74	0.63	28.05	1.20	1.31	0.11	39.05	84.30	199	1.88	0.01	0.618	0.007
Dol#6	0.26	13.05	0.58	27.83	3.72	0.62	0.07	39.27	85.41	197	5.80	0.02	1.20	0.02

b.d.: below detection limit. *mol% of total cations.

793

794

Table 2

RSF values of synthetic dolomites and calcite.

Sample	Average RSF	2SD	*N*
Days 1-3			
Cal#0	0.709	0.022	5
Dol#0	0.786	0.023	5
Dol#2	0.778	0.060	10
Dol#6	0.820	0.039	9
Day 4			
Cal#0	0.719	0.063	3
Dol#0	0.824	0.021	3
Dol#2	0.861	0.040	3
Dol#6	0.884	0.047	3

795

796

797

Table 3

Mn-Cr isotope systematics of Ivuna dolomite grains.

Measurement ID	Mg*	Ca*	Mn*	Fe*	RSF	Error**	$^{55}Mn/^{52}Cr$	Error**	$\delta^{53}Cr$ (‰)	Error**
Ivuna-H2 dolomite #7-1	42.8	47.1	6.9	3.2	0.797	0.052	63802	7193	2411	596
Ivuna-H2 dolomite #7-2	42.2	46.9	7.6	3.2	0.797	0.052	514	34	21	20
Ivuna-H2 dolomite #7-3	45.3	49.9	1.1	3.6	0.800	0.053	39820	6727	1268	787
Ivuna-H2 dolomite #7-4	46.3	49.0	1.2	3.6	0.800	0.053	49738	11152	1578	1172
Ivuna-H2 dolomite #7-5	45.2	49.5	2.2	3.1	0.796	0.052	12324	1106	419	234
Ivuna-H2 dolomite #7-6	43.9	51.1	1.6	3.4	0.865	0.049	5439	403	114	159
Ivuna-H2 dolomite #7-7	43.0	46.1	7.6	3.4	0.864	0.049	55812	5622	2375	536
Ivuna-H2 dolomite #3-1	43.3	49.9	4.0	2.8	0.794	0.052	57435	5512	2024	420
Ivuna-H2 dolomite #3-2	43.8	49.1	4.0	3.1	0.796	0.052	24724	2040	689	211

*mol% of total cations. **95% confidence interval.

798

Figure captions

Fig. 1. XRD patterns of an experimental product after heating at 300-340 °C (Dol#0: crystalline dolomite) and amorphous Ca- and Mg-carbonate (ACMC) after dehydration. These results show that the ACMC remained amorphous after dehydration, and that the ACMC crystallized to dolomite after heating at 300-340 °C. No other phase can be identified. For phase identification and indexing of the analyzed samples, crystallographic open database (COD) files were used.

Fig. 2. Backscattered electron image (BEI) of Dol#0. No impurity was found, which supports the results of the XRD analysis. Dol#0 as well as other synthetic dolomites and calcite appear a little porous, resulting in the low totals (83 to 92 wt%) of the EPMA analysis (Table 1).

Fig. 3. MnO and Cr_2O_3 abundances in Cal#0 (a), Dol#0 (b), Dol#2 (c), and Dol#6 (d) measured using EPMA. Typical 2σ errors based on counting statistics are shown by crosses. The variability of the data is well-explained by the Poisson distribution, and therefore, any heterogeneity regarding Mn and Cr concentrations cannot be recognized throughout the sample mount.

Fig. 4. Variability of the relative sensitivity of factor (RSF) of synthetic dolomites and calcite (left axis) and the $^{55}Mn^{+}/^{52}Cr^{+}$ ion intensity ratio of Ivuna-H2 dolomite (right axis) with time during a single analysis. The $^{55}Mn^{+}/^{52}Cr^{+}$ ratio is shown as a moving average

821 of 11 points (cycles) because the $^{52}Cr^{+}$ count rates of the Ivuna dolomite are very low.
822 The result of San Carlos olivine is also shown as reference. The RSF values of each
823 sample are the averages of multiple measurements in days 1-3. The RSF values of the
824 synthetic dolomites and calcite decrease with time by 10s of %, which is in contrast to
825 what was observed for San Carlos olivine. The similar time dependency can be observed
826 for the Ivuna dolomite. Note that the difference between the RSF values of Dol#0, Dol#2,
827 and Dol#6 is most pronounced at the beginning of the measurements but is smaller at the
828 end.

829

830 **Fig. 5.** RSF values of the synthetic dolomites and calcite in days 1-3 (a) and day 4 (b)
831 shown as a function of their Fe contents. The RSF values are the averages of 120 cycles
832 in each measurement. The reproducibility of the RSF values is as good as 3-5% for Dol#0,
833 Dol#6, and Cal#0 in days 1-3 even if the $^{55}Mn^{+}/^{52}Cr^{+}$ ratios changed drastically during a
834 single analysis (Fig. 4). For Dol#2, the reproducibility of the RSF values is ~8%, slightly
835 worse that the other synthetic dolomites and calcite, but the reason is unclear. The linear
836 regression (solid line) for the synthetic dolomites is drawn with the 95% confidence
837 interval of the inferred RSF value at a given Fe content (dashed line). For reference, the
838 RSF values of Cr-implanted dolomite reported by McCain et al. (2023), which are
839 commonly higher than our RSF values, are also shown with exponential regression.

840

841 **Fig. 6.** Mn-Cr isochron diagram (a) and $\delta^{53}Cr$ vs. $1/^{52}Cr$ diagram (b) of Ivuna-H2 dolomite
842 #7 and #3. The $\delta^{53}Cr$ values of Ivuna-H2 dolomite #7 and #3 correlate with $^{55}Mn/^{52}Cr$
843 ratios, suggesting *in-situ* decay of ^{53}Mn. A much weaker correlation in (b) than in (a)

844 excludes a possibility that this correlation represents a mixing line. The data obtained in
845 days 1-3 and in day 4 are shown together, and both the dataset plot on a single regression
846 line in (a). The slope of the regression line corresponding to the initial $^{53}Mn/^{55}Mn$ ratio,
847 $(^{53}Mn/^{55}Mn)_0$, at the isotopic closure is $(3.95 \pm 0.49) \times 10^{-6}$ (95% confidence interval).
848 The y-intercept, which corresponds to the initial $\delta^{53}Cr$ value, is 1± 20‰.

Fig. 1

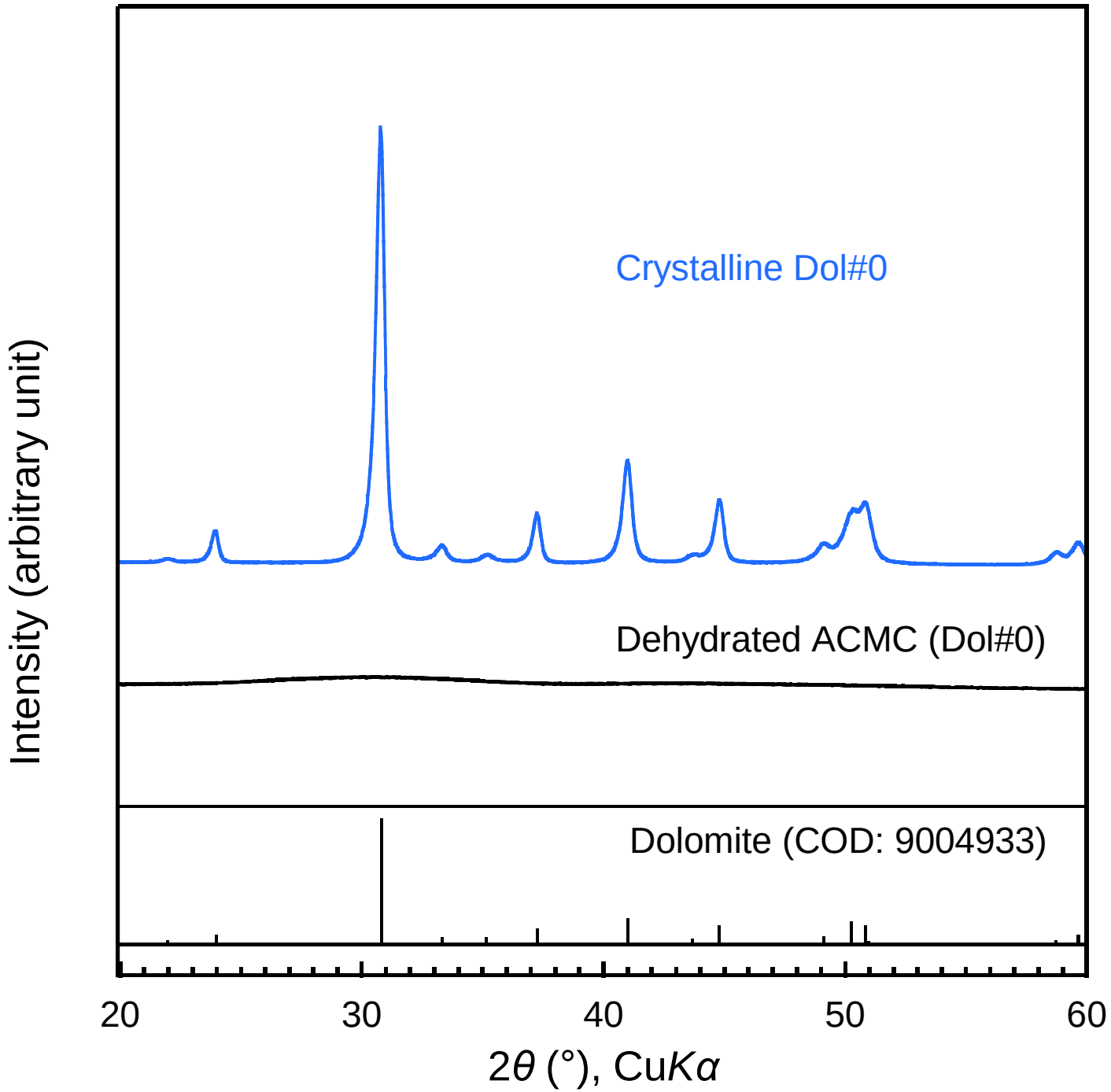

Crystalline Dol#0
Dehydrated ACMC (Dol#0)
Dolomite (COD: 9004933)
Intensity (arbitrary unit)
20
30
40
50
60
2θ (°), CuKα

Fig. 2

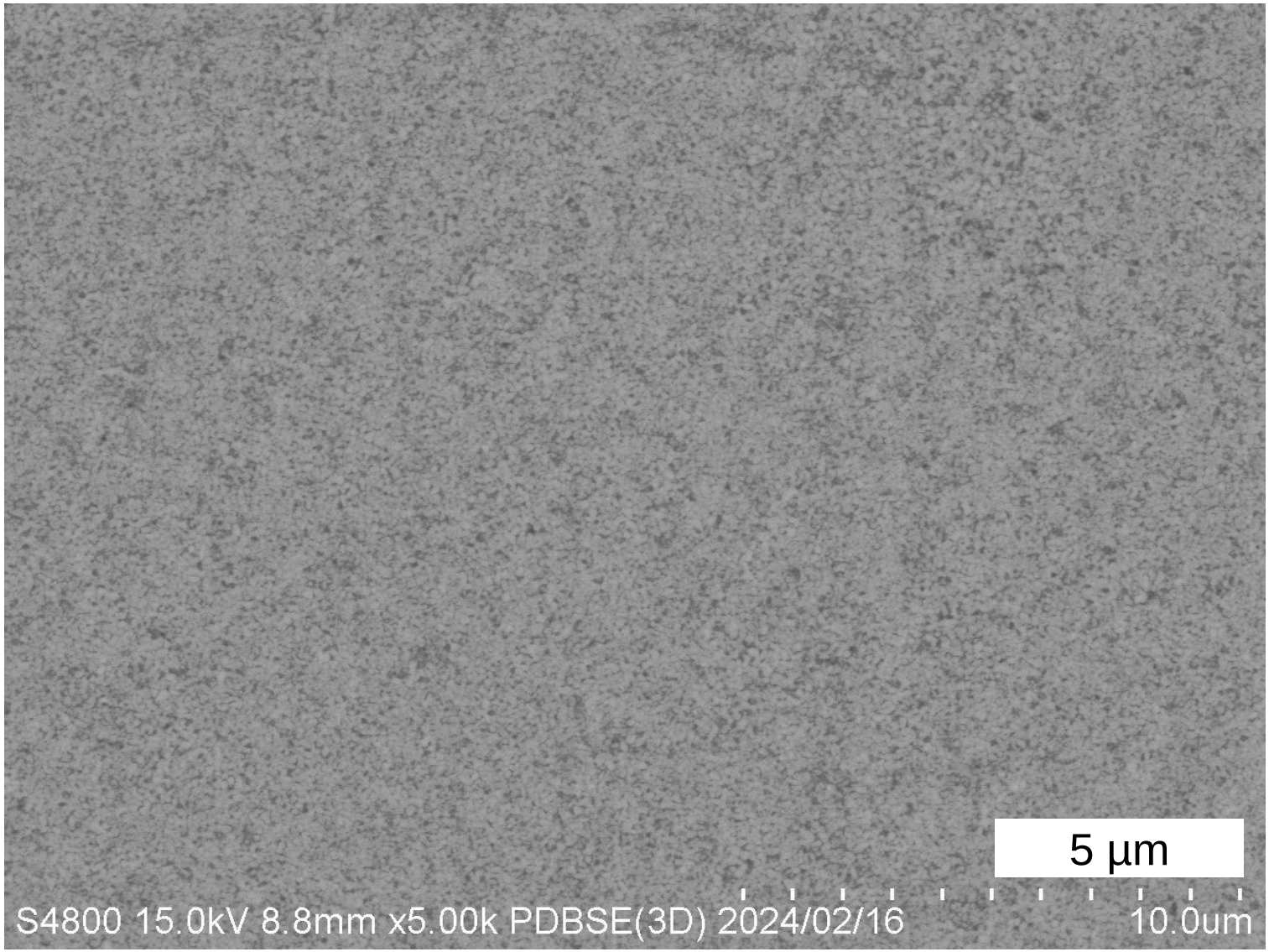


Fig. 3

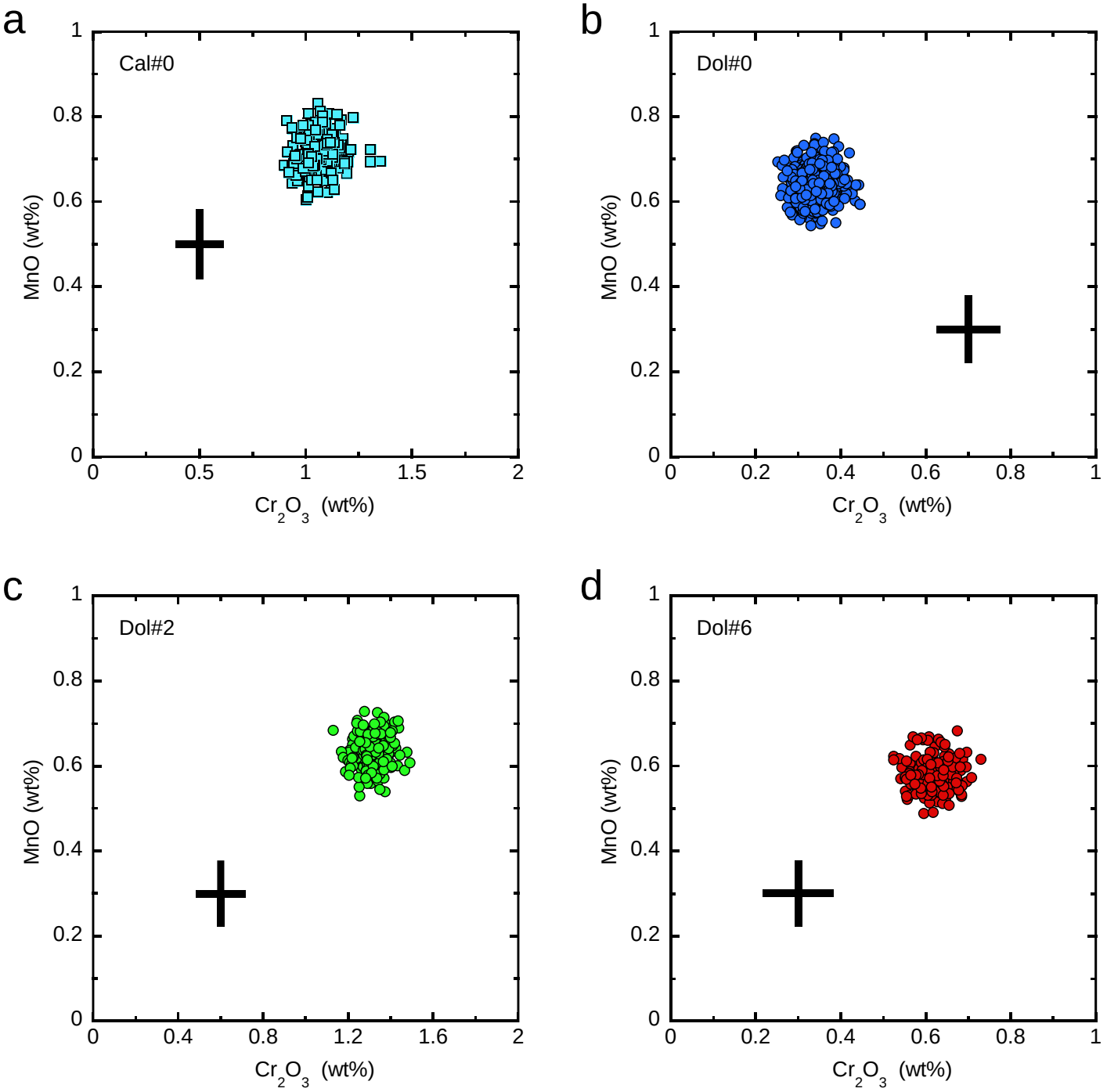

a
Cal#0
MnO (wt%)
Cr_2O_3 (wt%)
b
Dol#0
MnO (wt%)
Cr_2O_3 (wt%)
c
Dol#2
MnO (wt%)
Cr_2O_3 (wt%)
d
Dol#6
MnO (wt%)
Cr_2O_3 (wt%)

Fig. 4

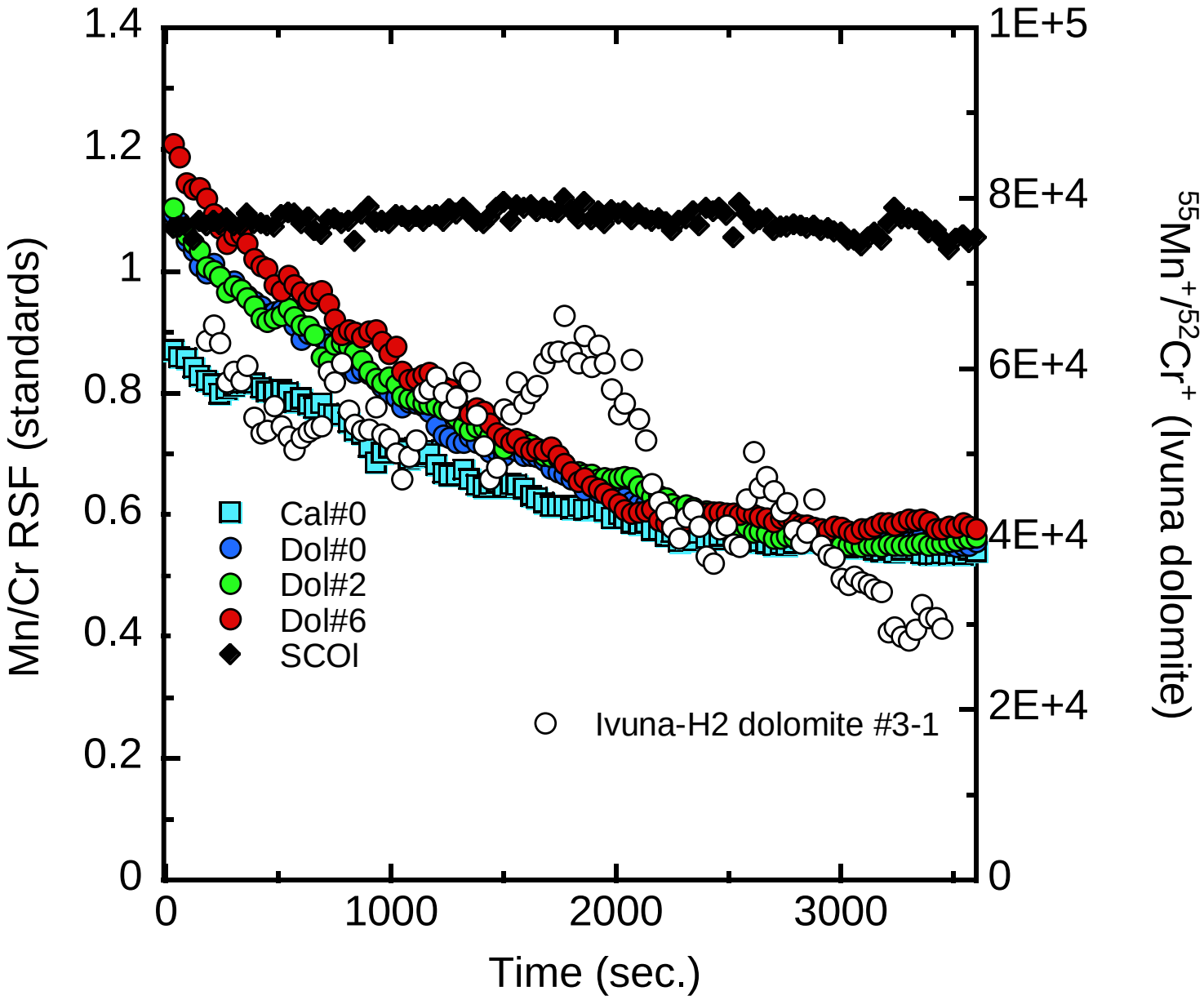

1.4
1.2
1
0.8
0.6
0.4
0.2
0
Mn/Cr RSF (standards)
1E+5
8E+4
6E+4
4E+4
2E+4
0
$^{55}Mn^{+}/^{52}Cr^{+}$ (Ivuna dolomite)
0
1000
2000
3000
Time (sec.)
Cal#0
Dol#0
Dol#2
Dol#6
SCOl
Ivuna-H2 dolomite #3-1

Fig. 5

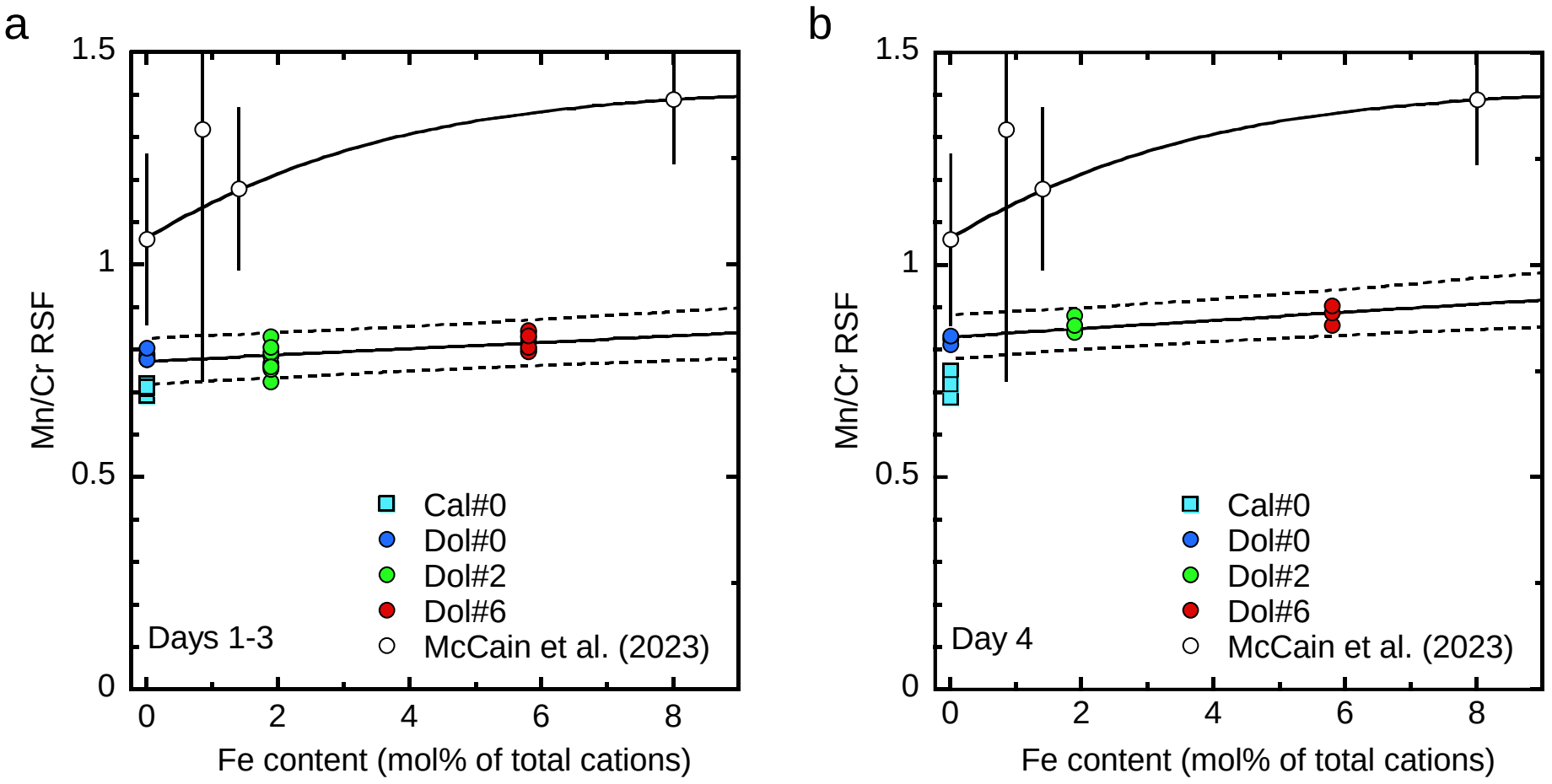
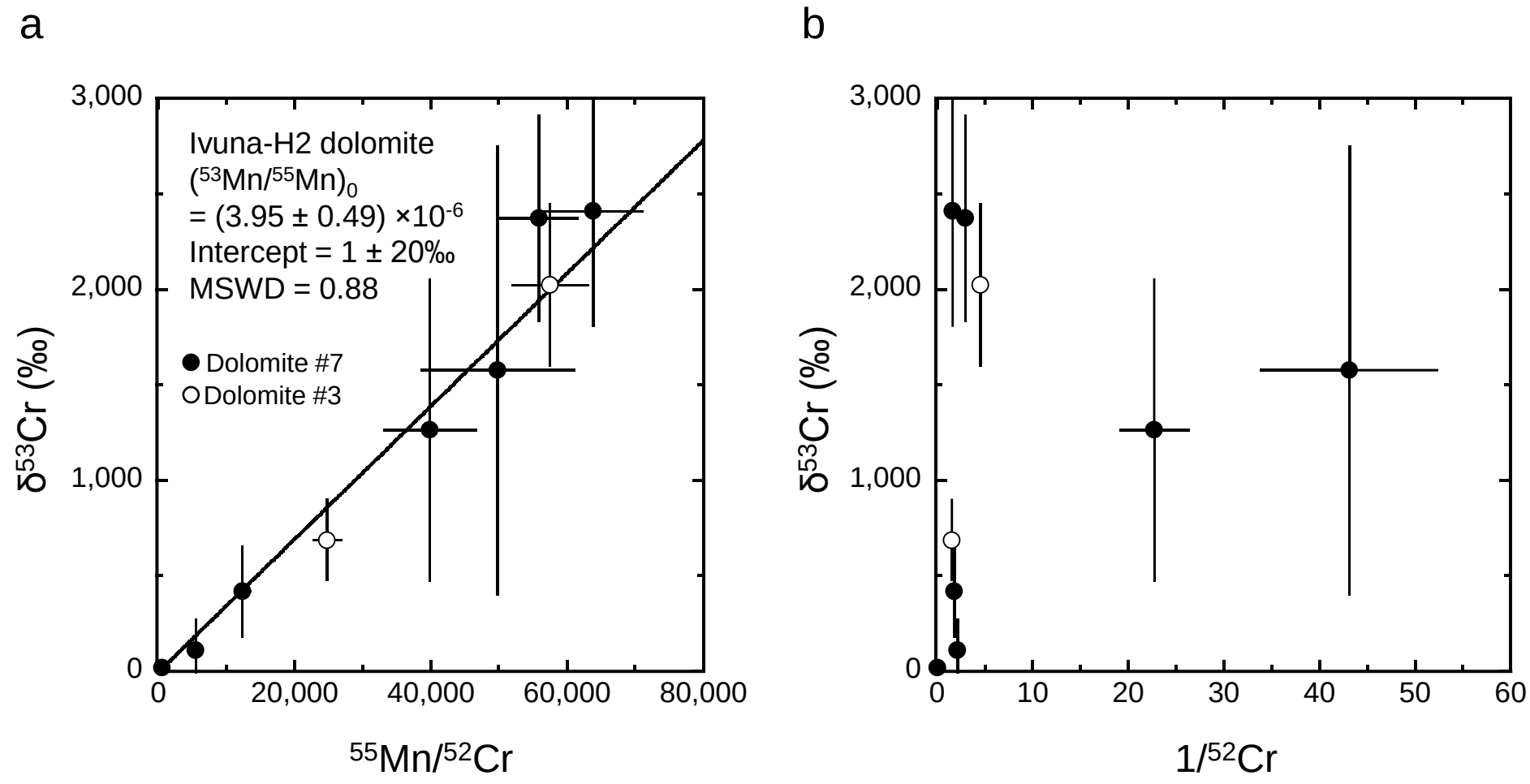

a
b
1.5
1
0.5
0
Mn/Cr RSF
0
2
4
6
8
Fe content (mol% of total cations)
Cal#0
Dol#0
Dol#2
Dol#6
McCain et al. (2023)
Days 1-3
Day 4

Fig. 6


a
b
Ivuna-H2 dolomite
(53Mn/55Mn)0
= (3.95 ± 0.49) ×10-6
Intercept = 1 ± 20‰
MSWD = 0.88
Dolomite #7
Dolomite #3
δ53Cr (‰)
55Mn/52Cr
1/52Cr
0
1,000
2,000
3,000
0
20,000
40,000
60,000
80,000
10
30
40
50
60